# Fabrication of Monodisperse Magnetite Hollow Spheres

**Peng Hu, Lingjie Yu, Ahui Zuo, Chenyi Guo, and Fangli Yuan***

*State Key Laboratory of Multi-phase Complex System, Institute of Process Engineering, Chinese Academy of Sciences, Beijing 100190, China*

*Received: July 21, 2008; Revised Manuscript Received: November 17, 2008*

Monodisperse $Fe_3O_4$ hollow spheres with average diameter of 400 nm and shell thickness of 60 nm were prepared through a one-pot solvothermal process with the presence of $NH_4Ac$ as the structure-directing agent, and a novel gas-bubble-assisted Ostwald ripening process was proposed to explain the formation of hollow structures. According to this mechanism, hollow $Fe_3O_4$ and $MnFe_2O_4$ ferrite microspheres with controlled particle size were obtained using urea and ammonia as the structure-directing agents, and porous $Fe_3O_4$ spheres with particle size of 100 nm and pore size of 10 nm were obtained by the assistance of bicarbonate of ammonia. X-ray diffraction, scanning electron microscopy, transmission electron microscopy, and high-resolution transmission electron microscopy were used to characterize the structure of synthesized products, and the magnetic property investigation shows that the hollow microspheres exhibit a ferromagnetic behavior and possess a higher saturation magnetization ($M_s$) than that of the solid microspheres.

## 1. Introduction

The design and synthesis of functional materials with controlled shapes and desired morphology have stimulated great research interest because of their novel properties and potential applications in nanodevices.[1−6] In the past decade, significant progress in the synthesis of functional materials has been achieved, and many novel structures, including tubes, rods, octahedral, and self-assemble structures with size from several to hundreds of nanometers, have been developed.[7−11] Among nanomaterials with different structures, hollow magnetic spheres have received much attention for their peculiar properties and potential applications in high-density magnetic data storage, ferrofluids, spin electronic devices, magnetic resonance imaging, and biomaterials diagnostics.[12−17] For example, $Fe_3O_4$, as one of the most important magnetite materials, has been considered an ideal material for biological magnetic applications such as targeted drug delivery for antitumor therapy,[18] hyperthermia treatment of cancers,[19] enzymatic assays,[20] and activity agent for medical diagnostics[21] because of its good hydrophilic, biocompatible, nontoxicity properties, and high chemical stability.[22,23] Moreover, the hollow interiors may potentially serve as tunable channels to carry drugs, and the hollow magnetic spheres might be used for encapsulation of various guest molecules for specific drug delivery, which broaden their applications in the biomedical field.

The success in synthesis of magnetite particles with a narrow size distribution could be retrospect to the early 1980s,[24] and the monodisperse ferrite spheres have also been obtained by various synthetic methods.[25−29] However, the approaches to fabricate hollow ferrite monodisperse particles were developed in recent years pursued by their scientific and technological importance. Template-assisted synthesis is a facile way to prepare hollow structures, and different materials such as silica spheres, polystyrene latex spheres, and polymer micelles have been used as templates to direct the formation of hollow spheres.[30−32] The procedure involves deposition of thin shells of nanoparticles on the template followed by selective removal of the template, and the products obtained from the complex processes often relate to poorly defined pore size/shape and high cost.[33,34] Other synthetic strategies, such as reverse micelle transition, the Ostwald ripening process, have also been used to prepare hollow ferrite microspheres.[33,35−38] However, most of these approaches are focused on the synthesis of ferrite monodisperse particles with a narrow size distribution and well defined pore size/shape but limited to the fabrication of monodisperse ferrite nanospheres with tunable diameter and cavity. The development of a facile and economic method for the synthesis of monodisperse ferrite spheres with tunable structure would greatly promote their applications in biomedical field.

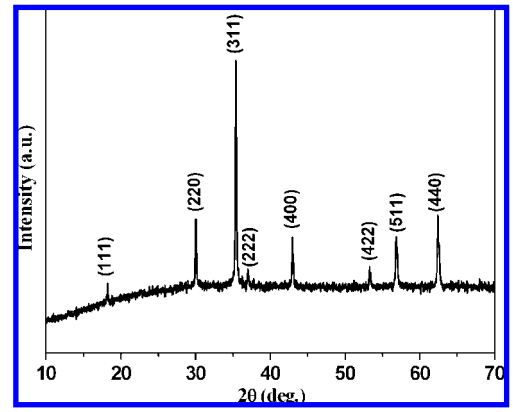


**Figure 1.** XRD pattern of as-synthesized $Fe_3O_4$ hollow microspheres.

Herein, we report a facile solvothermal reduction method for preparation of monodisperse $Fe_3O_4$ hollow spheres by modifying the reaction to prepare solid $Fe_3O_4$ microspheres.[39] In our system, the ammonium salts were introduced to replace the NaAc, and they were crucial to the formation and transformation of the hollow interiors. Furthermore, this one-pot synthetic strategy is general for the preparation of a series of monodisperse

* Corresponding author. Phone: +86-10-82627058. Fax: +86-10-62561822. E-mail: flyuan@home.ipe.ac.cn.

10.1021/jp806406c CCC: $40.75 
Published on Web 12/31/2008

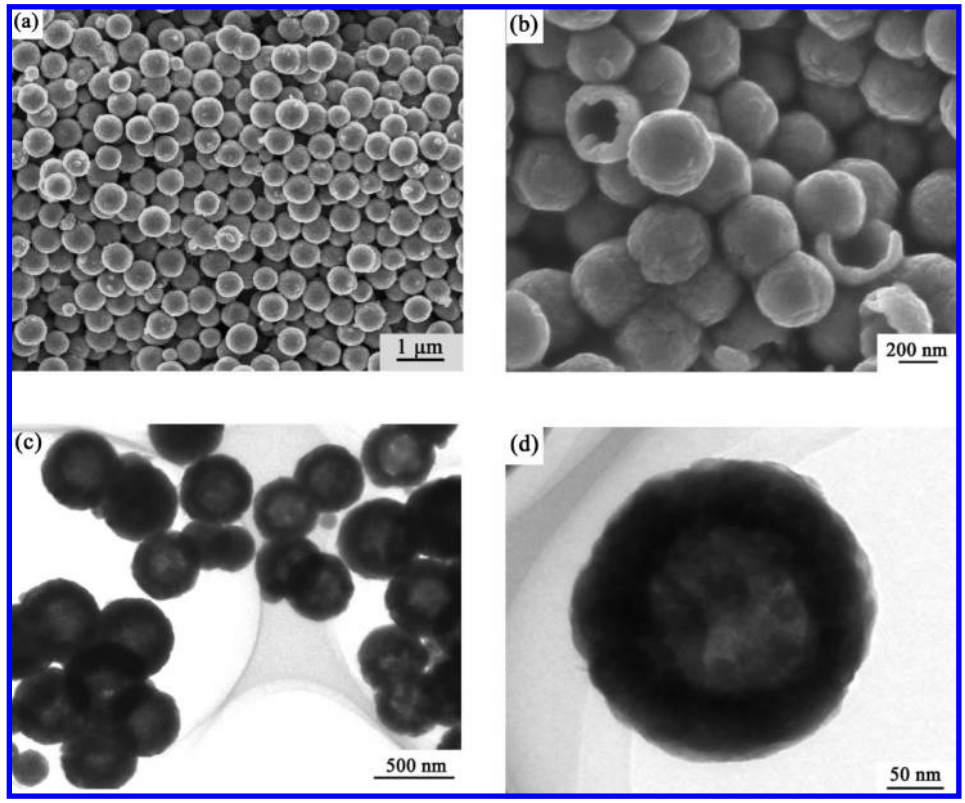


**Figure 2.** (a) Low magnification and (b) high magnification SEM images of $Fe_3O_4$ hollow microspheres; (c) low magnification TEM image and (d) enlarged TEM image of an individual $Fe_3O_4$ hollow sphere

ferrite hollow spheres ($MFe_2O_4$, M = Mn, Co, Zn) with tunable diameters and interiors, which makes it possible to further investigate their unique properties and potential applications.

## 2. Experimental Section

**2.1. Preparation of the Monodisperse $Fe_3O_4$ Hollow Spheres.** All reagents are analytically pure and used as-received without further purification. In a typical experiment, 5 mmol $FeCl_3 \cdot 6H_2O$ was dissolved in 60 mL of ethylene glycol, followed by the addition of 0.05 mol $NH_4Ac$ under magnetic stirring to form a clear solution. The result mixture was transferred to a 100 mL Teflon-lined autoclave and then maintained at 200 °C for 12 h. After reaction, the autoclave was cooled to room temperature. The products were obtained by centrifuging and sequentially washing with water and ethanol for several times and then dried in a vacuum oven at 60 °C for 6 h.

**2.2. Sample Characterization.** X-ray diffraction (XRD) patterns were recorded with a Philips X'Pert PRO MPD X-ray diffractometer using Cu $K_\alpha$ radiation. Transmission electron microscope (TEM) images were taken on a Hitachi H-800 transmission electron microscope. High resolution (HR) TEM images were obtained using a JEOL JEM-2011 transmission electron microscope. Scanning electron microscopy (SEM) images were taken with a JSM-6700F scanning electron microscope. Magnetic investigation was carried out on a LDJ-9600 vibrating sample magnetometer (VSM).

## 3. Results and Discussion

Figure 1 shows the XRD pattern of sample synthesized at 200 °C for 12 h. All the diffraction peaks can be well indexed to the magnetic cubic structure of $Fe_3O_4$ (JCPDS 79−0419) with lattice constants of $a$ = 8.396 Å, and no peaks due to the hematite and other impurities were detected in the XRD patterns, indicating the formation of pure magnetic products. The sharp and strong diffraction peaks also confirm the well crystallization of the products.

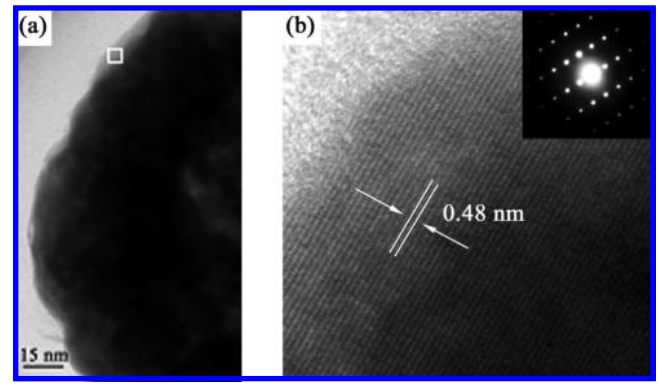


**Figure 3.** (a) TEM image of part of a single $Fe_3O_4$ microsphere and (b) corresponding HRTEM image recording from the boxed region in (a)

The morphology and structure of obtained products were investigated by SEM and TEM as shown in Figure 2. Figure 2a gives the representative SEM image of as-synthesized products, which suggests that the products consist of a larger quantity of spheres with an average diameter of ca. 400 nm. The magnified image shown in Figure 2b exhibits detailed morphology of the obtained products, indicating the formation of uniform, regular microspheres, and some broken spheres could also be observed in the image, confirming that the spheres have a hollow interior. In addition, it can also be observed from the surface of the particles that the spheres are composed of some much smaller particles. The hollow structure is further

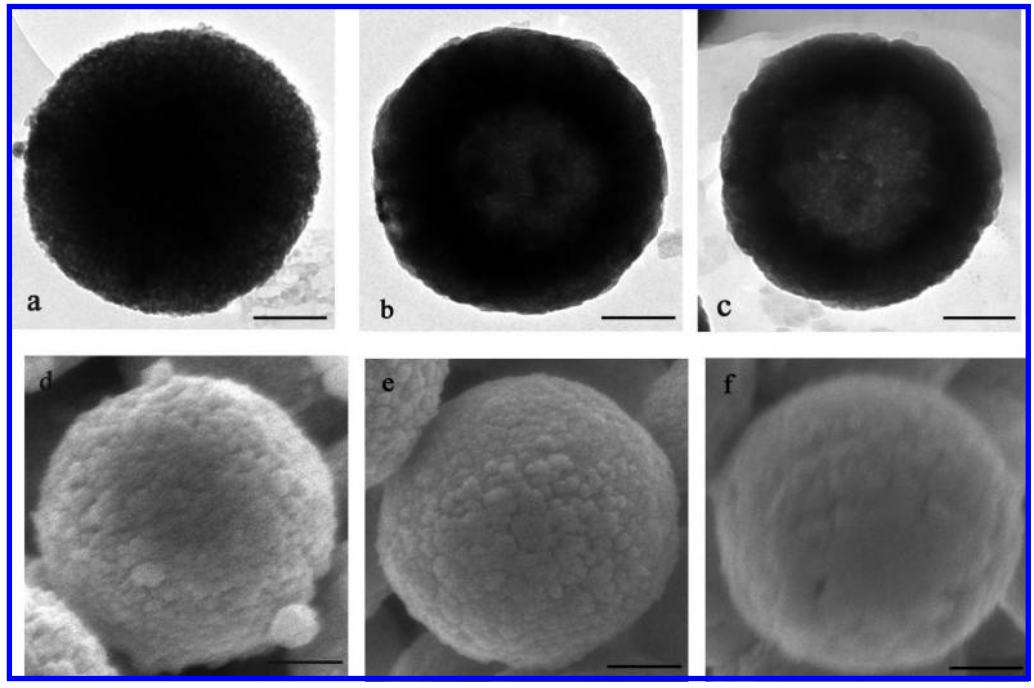


**Figure 4.** TEM images of products synthesized with different reaction time: (a) 8 h, (b) 10 h, (c) 12 h and corresponding SEM images of d, e, and f. Scale bar: 300 nm.

investigated by the TEM image as shown in Figure 2c, and the intensive contrast between the black margin and the bright center of the particles confirms the existence of hollow structures in the resulting spheres, consistent with the SEM observation. Figure 2d gives the typical TEM image of an individual particle, and the average diameter and shell thickness could be determined as 400 and 60 nm, respectively.

More detailed structural information of synthesized products was provided by the high-resolution TEM analysis, and Figure 3b shows the HRTEM image and the corresponding selected area electron diffraction (SAED) taken from an individual hollow particle as shown in Figure 3a (marked by a rectangle). The clearly atomic lattice fringes could be observed, and the measured spacing of the crystallographic planes is about 0.48 nm, which is close to the (111) lattice planes of $Fe_3O_4$ crystal. The HRTEM image and the SAED pattern reveal that the hollow microspheres are composed of single crystalline nanocrystallites.

The influences of experiment parameters on the structure of final products were investigated systemically, and the results show that the temperature, time, and the amount of $NH_4Ac$ play key roles in the formation of monodisperse $Fe_3O_4$ hollow spheres. When the temperature decreases to 190 °C, only brown precipitates, instead of black $Fe_3O_4$, were obtained after reaction for 12 h, which is the same as the products synthesized at 200 for 8 h. Although the higher temperature (such as 210 °C) favors the formation of $Fe_3O_4$, the hollow microspheres with a broad diameter distribution and rough surface were predominant in the final products (see Supporting Information). In addition, the amount of $NH_4Ac$ is also critical to the formation of $Fe_3O_4$ hollow structures. Although ethylene glycol is reported to be a strong reducing agent in the polyol process to synthesis metal or metal oxide nanoparticles,[39,40] no resulting products were obtained under the same experiment conditions without $NH_4Ac$. The yellow precipitates were synthesized by introducing a small quantity of $NH_4Ac$ to the system, and the color of obtained products changes to brown with increase of the amount of $NH_4Ac$. The pure $Fe_3O_4$ could be obtained when $NH_4Ac$ exceeds 0.04 mol without changing other parameters.

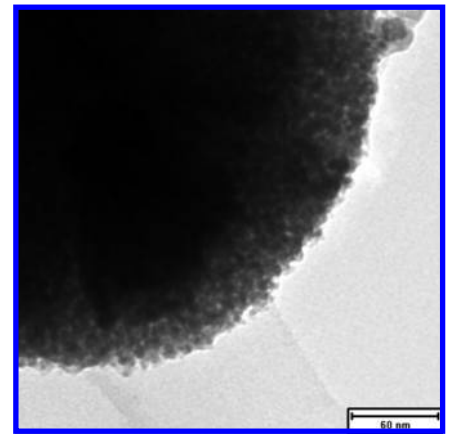


**Figure 5.** The representative high-magnification TEM images of spherical aggregate synthesized at 200 °C for 8 h.

To investigate the evolution process of the core evacuation, time-dependent experiments were conducted, and Figure 4 gives the TEM and SEM images of products synthesized at different reaction times. It is indicated that there are obvious changes for the surface morphology and interior cavity of the microspheres. From Figure 4a we can see that spherical particles with a solid core are obtained within the first reaction time of 8 h, the microsphere is then followed by a solid core evacuation, and a hollowing effect is observed for those with a longer reaction time of 10 h (Figure 4b). The inner space of the spheres is further increased in comparison to the shell (darker spherical circle) when the reaction time is longer (12 h, Figure 4c), indicating continued evacuation of central cavities. During this process, there is no apparently increase for the particle sizes with the increase of reaction time, but there is a clear change in their surface morphology. Figure 4d−f give the detailed surface morphology of the products obtained with the corresponding reaction time. After the first reaction time of 8 h, spherical particles with a rough surface are observed, which indicates that the microsphere is formed by aggregation of small

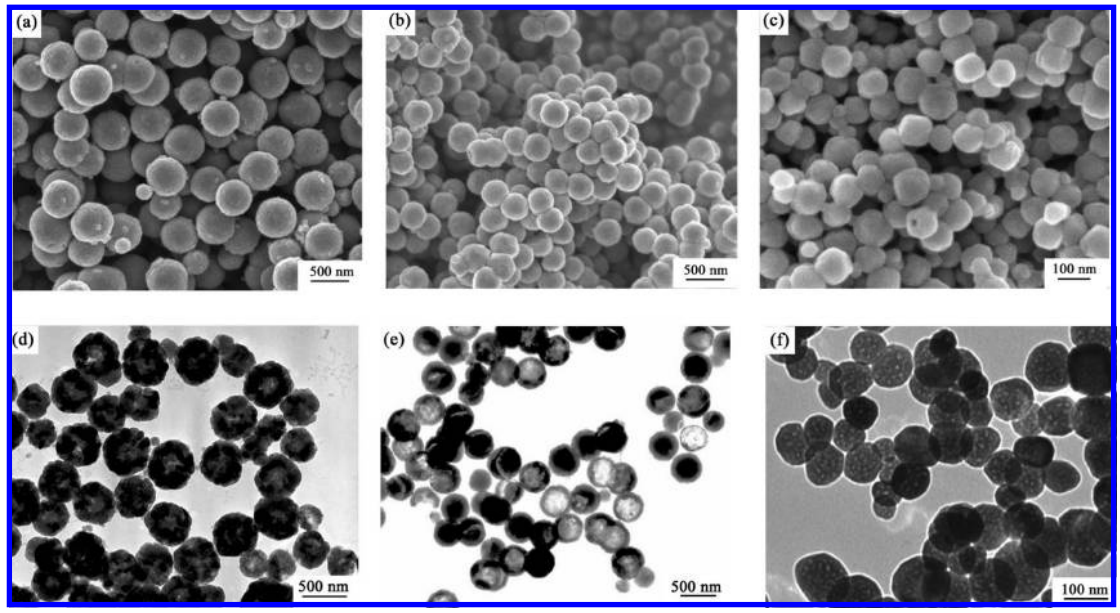


**Figure 6.** SEM images of products synthesized with the assistance of (a) urea, (b) ammonia, (c) bicarbonate of ammonia and the corresponding TEM images in d, e, and f.

nanocrystallites (Figure 4d). When the reaction time is increased up to 10 h, the aggregate begins to transform into a smooth microsphere as shown in Figure 4e. Further prolonging the reaction time leads to a more compact and smooth surface of the microsphere (Figure 4f).

Regarding the formation process of hollow interiors, it is recognized that the Ostwald ripening should be the underlying mechanism for the formation of hollow microspheres. Generally, Ostwald ripening involves the formation of aggregates with primary crystallites and is followed by the gradual outward migration of crystallites through a recrystallization process due to the energy difference among them.[41] First, the fresh-formed nanoparticles are thermodynamically favored to aggregate together to form solid spheres, and then the inner crystallites of the aggregate go through the mass transfer to the outer shell by a dissolution−recrystallization process at the cost of the small ones, which have higher surface energies and solubility than the larger ones. With a lengthened ripening process, outward migration of crystals would result in continued expansion of interior space within the original aggregates, and the inner space of the spheres is further increased. The evolution of the building blocks in the spherical surface shown in Figure 4d−f also proved the symmetric ripening process.

Although the hollowing process could be well explained by Ostwald ripening, it is noted that the time needed to form hollow structures in our process using $NH_4Ac$ as the structure-directing salt is much shorter and the hollow interiors are much more distinct than that in other ripening systems (generally, the time needed for structure evolution from solid to hollow structure by Ostwald ripening process is longer than 24 h).[41−43] Recent research shows that the hollow $Fe_3O_4$ microspheres could also be obtained in ethylene glycol solution by Ostwald ripening process using NaAc as the structure-directing salt at 200 °C for prolonging the reaction time to 30 h.[36] These results reveal that the core evacuation could be occurred using different assisting regents in ethylene glycol system, but the hollowing effect is distinguishing for different structure-directing agents with the same reaction time, and the hollowing process could be significantly accelerated with the assistance of $NH_4Ac$ as the structure-directing salt. In addition, our previous investigations revealed that $NH_4Ac$ functioned as an assistant-reducing agent in the synthesis process, and no products were obtained in ethylene glycol solution without the addition of $NH_4Ac$. Accordingly, $NH_4Ac$ should play a key role in the synthesis of $Fe_3O_4$ hollow microspheres. As we all know, $NH_4Ac$ is a weak-acid−weak-base salt and is easily hydrolyzed at a high temperature in solution, and trace amount of water was present in our system originating from the crystalline water of $FeCl_3 \cdot 6H_2O$. It is reasonable that hydrolysis of $NH_4Ac$ occurred in the synthesis process, and possible chemical reactions in this system for the synthesis of hollow $Fe_3O_4$ microspheres are proposed as follows.

$$NH_4Ac + H_2O \rightleftarrows HAc + NH_3 \cdot H_2O \quad (1)$$

$$NH_3 \cdot H_2O \rightleftarrows NH_4^+ + OH^- \quad (2)$$

$$Fe^{3+} + 3OH^- \rightarrow Fe(OH)_3 \quad (3)$$

$$Fe^{2+} + 2OH^- \rightarrow Fe(OH)_2 \quad (4)$$

$$2Fe(OH)_3 + Fe(OH)_2 \rightarrow Fe_3O_4 + 4H_2O \quad (5)$$

Under hydrothermal conditions, $NH_4Ac$ was hydrolyzed into HAc and $NH_3 \cdot H_2O$, and partial $NH_3 \cdot H_2O$ was evaporated and formed little gaseous bubbles. As a simple confirmation for this reaction, the postreaction solution was immediately detected by gas chromatography to analyze the gas released from the solution, and the results provided the amount of generated gas during the reaction (see Supporting Information). The fresh produced gaseous bubbles have high surface energy due to their small diameter (high curvature) and provide the heterogeneous nucleation center for newly formed nanoparticles to aggregate around the gas−liquid interface. The spherical aggregates are then formed by aggregation of original nanocrystallites nucleated on the gas−liquid interface to minimize the interfacial energy, and thus the bubbles were remaining in the interior of the aggregates.[44,45] Figure 5 gives the representative high-magnification TEM images of spherical aggregate synthesized at 200 °C for 8 h, which indicate that the aggregates are constructed of many small nanocrystals, and wormlike nanopores with pore size of several nanometers, can be seen clearly in the nanoc-

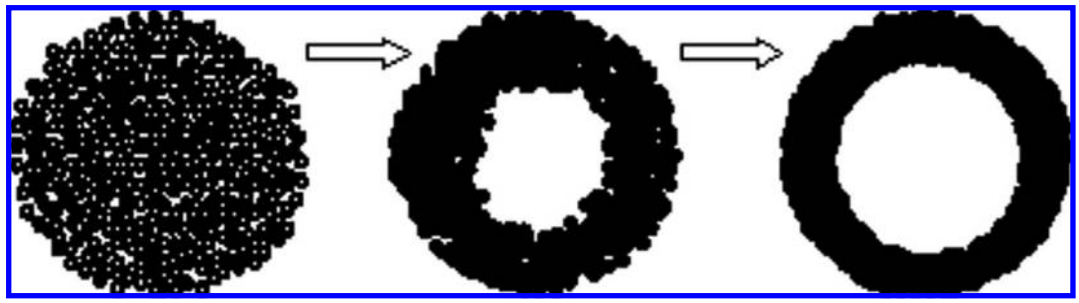

**Figure 7.** Schematic illustration of the process of obtaining magnetite hollow microspheres.

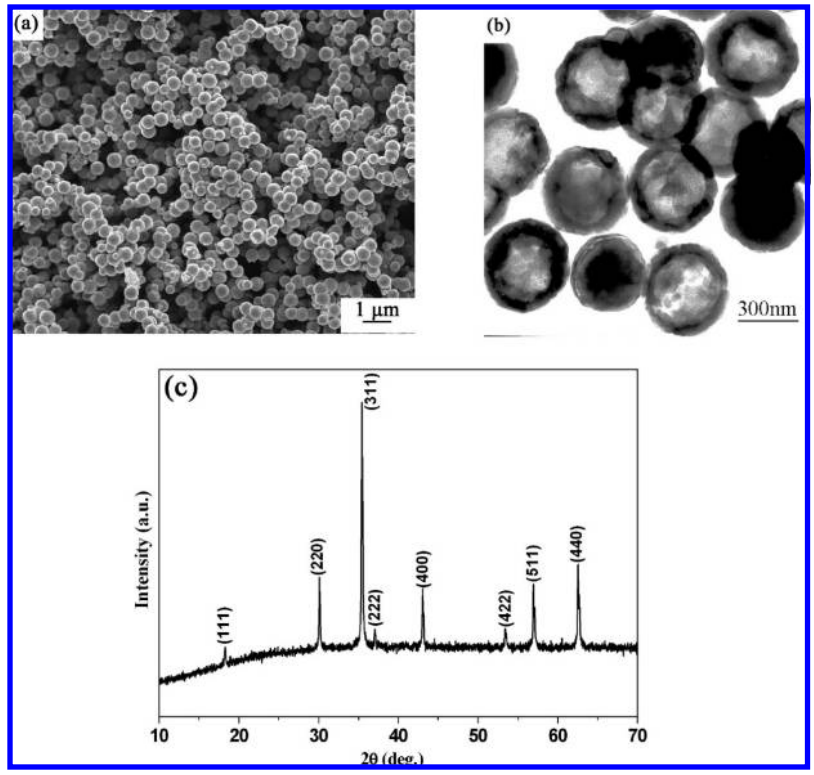


**Figure 8.** (a) SEM images, (b) TEM images, and (c) XRD pattern of synthesized $MnFe_2O_4$ hollow spheres.

rystallites forming the spherical loose nanostructures. The wormlike nanopores are suggested to be evidence of gas bubbles in the aggregates. Since the original driving force for this ripening could be attributed to the intrinsic density variations inside the starting solid aggregates, the loosely packed crystallites in the shell would serve as starting growth sites for the subsequent recrystallization and speed up the mass transport. During the ripening process, the smaller crystallites located at central cores tend to relocate themselves to the shell, and the interior space continues to expand. The inner nanospace occupied by the bubbles is released and becomes part of the void space. As a result, the distinctly hollowing effect could be observed in a short reaction time. When anhydrous iron chloride was used as a starting material, the hydrolysis of $NH_4Ac$ was totally stopped and no hollow microspheres were obtained in the final products as proposed (see Supporting Information).

As indicated in above investigations, it is suggestive that Ostwald ripening is also associated with the chemical nature of ionic species in the solution during the synthesis. This point is further addressed in the following synthetic experiments. Different ammonium salts, including urea, ammonia, and bicarbonate of ammonia, were used as structure-directing agents, and they all could produce gas in the synthesis process. Figure 6 shows the representative images of products synthesized with different ammonium species. From the SEM images of Figure 6a, 6b, and 6c, we can see that monodisperse spheres are obtained in all cases, and the particle size is about 500, 400, and 100 nm, respectively. The hollow interior is further revealed by the TEM images as shown in Figure 6d and 6e, from which we can conclude that the products synthesized with the assistance of urea and ammonia as the structure-directing agents exhibit entirely hollow interiors similar to that obtained with the ammonium acetate as the structure-directing agent. However, the porous spheres were fabricated with the presence of bicarbonate of ammonia, and their diameter decreases to about 100 nm as shown in Figure 6f. Although the surface of the spheres is still very smooth, the intensive contrast in their interiors reveals the porous nature of the particles. The porous structure of magnetic spheres has not been reported previously, and its formation and properties need to be further investigated. These results indicated that the hollow spheres with tunable particle size and interior structure could be synthesized with different structure-directing salts and the fresh produced gas plays a key role in the morphology transformation of spherical aggregates from solid to hollow structure.

On the basis of above investigations, a gas-bubble-assisted Ostwald ripening process was proposed to explain the formation of microspheres with hollow structures. The formation of hollow

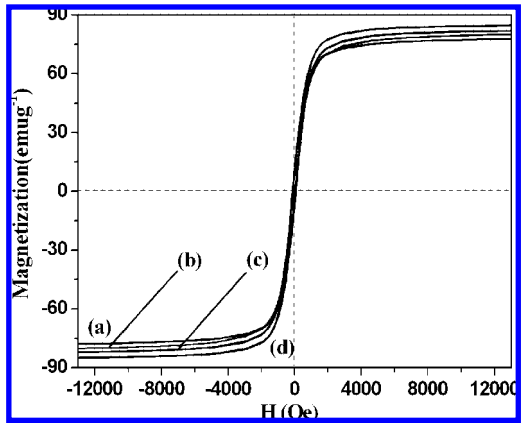


**Figure 9.** Room temperature magnetization curves for the as-obtained ferrite microspheres: (a) the solid $Fe_3O_4$ spheres, (b) the solid $MnFe_2O_4$ spheres, (c) the hollow $Fe_3O_4$ spheres, and (d) the hollow $MnFe_2O_4$ spheres.

spheres can divide into three stages. In the initial stage, original nanocrystallites nucleate on the interface of gaseous bubbles produced by hydrolysis and then aggregate to lose microspheres because of minimization of the interfacial energy. Because the crystallites are located in the inner cores, compared to those in the outer surfaces, they have higher surface energies and are easily dissolved. Thus, the subsequent crystallization process occurred using the nanocrystallites located in the shell as nucleation seeds, which leads to the durative growth of the shell at the expense of the cores inner spheres, and the results of this process are that the size of the core is reduced gradually while the hollow volume is enlarged. Finally, the hollow microspheres are formed with the complete depletion of the cores. Considering the inner space occupied by the bubbles, this solid evacuation process is faster than the general symmetric ripening. The schematic illustration of the formation process is shown in Figure 7.

This process could also be used to synthesize monodisperse $MFe_2O_4$ (M = Mn, Co, Zn) ferrite hollow microspheres (see Supporting Information). For $MnFe_2O_4$ as an example, the synthesis process was carried out by coprecipitation of $Mn^{2+}$ and $Fe^{3+}$ chlorides according to the stoichiometric ratio, and the products were obtained by the same treatment of the precursors. Figure 8 shows the typical images and XRD pattern of synthesized $MnFe_2O_4$. From the SEM image in Figure 8a we can conclude that the ferrite microspheres exhibit a narrow diameter distribution of about 400 nm, which is similar to that of $Fe_3O_4$ hollow microspheres. The hollow structure could also be confirmed by the TEM image showing in Figure 8b, and the monodisperse microspheres have a hollow interior with a shell thickness of ca. 60 nm. XRD investigation shown in Figure 8c confirms the formation of pure $MnFe_2O_4$ (JCPDS 73−1964), and the intensive diffraction peaks also reveal the well crystallization of the products.

The magnetic properties of as-obtained ferrite microspheres were investigated with a VSM at room temperature shown in Figure 9. The results show that all the ferrite microspheres exhibit ferromagnetic behavior, and the hollow microspheres possess a higher saturation magnetization ($M_s$) of ca. 84.7 emu $g^{-1}$ ($MnFe_2O_4$ hollow spheres) and 82.2 emu $g^{-1}$ ($Fe_3O_4$ hollow spheres) compared to that of 80.4 emu $g^{-1}$ ($MnFe_2O_4$ solid spheres) and 78.1 emu $g^{-1}$ ($Fe_3O_4$ solid microspheres) synthesized with the assistance of NaAc, which is contrary to values reported previously.[33] The difference in $M_s$ may be attributed to the change in particle size and interior structure, and more detailed investigations of the magnetic properties of these products are in progress. Accordingly, our work provides a facile way to adjust the magnetic properties of magnetic spheres, which makes them easily manipulated in an external magnetic field with different intensities and broadens their applications as biological magnetic materials.

## 4. Conclusions

In summary, monodisperse $Fe_3O_4$ hollow spheres with a size of 400 nm and shell thickness of 60 nm were prepared by a facile solvothermal process. A novel gas-bubble-assisted Ostwald ripening process was proposed to explain the formation of hollow structures, and the mechanism was confirmed using different ammonium salts. The hollow microspheres with a particle size of 400 and 500 nm were synthesized in the presence of urea and ammonia, while the porous spheres with a particle size of 100 nm were fabricated in the presence of $NH_4HCO_3$. The magnetism investigation shows that the as-prepared magnetite hollow spherical nanostructures exhibit a ferromagnetic behavior with a saturation magnetization higher than that of the solid spheres at room temperature. Accordingly, the present approach provides a convenient and effective way to prepare hollow ferrite micropheres and shows a high versatility for adjusting the size and inner structure of the particle, and the products have promising applications in biomedical fields.

**Acknowledgment.** The authors acknowledge the financial support from the National Nature Science Foundation of China (no. 50574083).

**Supporting Information Available:** A list of SEM and TEM images of the products synthesized under different experiment conditions. This material is available free of charge via the Internet at http://pubs.acs.org.

## References and Notes

(1) Rabani, E.; Reichman, D. R.; Geissler, P. L.; Brus, L. E. *Nature* **2003**, *426*, 271.
(2) Sun, S. *Adv. Mater.* **2006**, *18*, 393.
(3) Duan, X.; Huang, Y.; Cui, Y.; Wang, J.; Lieber, C. M. *Nature* **2001**, *409*, 66.
(4) Wang, X. D.; Song, J. H.; Liu, J.; Wang, Z. L. *Science* **2007**, *316*, 102.
(5) Empedocles, S. A.; Neuhauser, R.; Bawendi, M. G. *Nature* **1999**, *399*, 126.
(6) Lu, Y.; Xiong, H.; Jiang, C. X.; Xia, Y. N. *J. Am. Chem. Soc.* **2003**, *125*, 12724.
(7) Liu, J.; Xue, D. F. *Adv. Mater.* **2008**, *20*, 2622.
(8) Wang, X. D.; Summers, C. J.; Wang, Z. L. *Nano Lett.* **2004**, *4*, 423.
(9) Guo, Q. X.; Zhao, Y. S.; Mao, W. L.; Wang, Z. W.; Xiong, Y. J.; Xia, Y. N. *Nano Lett.* **2008**, *8*, 972.
(10) Kar, S.; Santra, S. *J. Phys. Chem. C* **2008**, *112*, 8144.
(11) Yan, C. L.; Xue, D. F. *Adv. Mater.* **2008**, *20*, 1055.
(12) Cao, S. W.; Zhu, Y. J.; Ma, M. Y.; J. Li, L.; Zhang, L. *J. Phys. Chem. C* **2008**, *112*, 1851.
(13) Hyeon, T.; Lee, S. S.; Park, J.; Chung, Y.; Na, H. B. *J. Am. Chem. Soc.* **2001**, *123*, 12798.
(14) Woo, K.; Lee, H. J.; Ahn, J.; Park, Y. S. *Adv. Mater.* **2003**, *15*, 1761.
(15) Wang, Y.; Teng, X.; Wang, J.; Yang, H. *Nano Lett.* **2003**, *3*, 789.
(16) Caruso, F.; Spasova, M.; Susha, A.; Giersig, M.; Caruso, R. A. *Chem. Mater.* **2001**, *109*, 1851.
(17) Kim, D. K.; Zhang, Y.; Kehr, J.; Klason, T.; Bjelke, B.; Muhammed, M. *J. Magn. Magn. Mater.* **2001**, *225*, 256.
(18) Dobson, J. *Drug Dev. Res.* **2006**, *67*, 55.
(19) Mornet, S.; Vasseur, S.; Grasset, F.; Duguet, E. *J. Mater. Chem.* **2004**, *14*, 2161.
(20) Mirzabekov, T.; Kontos, H.; Farzan, M.; Marasco, W.; Sodroski, J. *Nat. Biotechnol.* **2000**, *18*, 649.
(21) Koh, I.; Wang, X.; Varughese, B.; Isaacs, L.; Ehrman, S. H.; English, D. S. *J. Phys. Chem. B* **2006**, *110*, 1553.

(22) Woo, K.; Hong, J.; Choi, S.; Lee, H.; Ahn, J.; Kim, C. S.; Lee, S. W. *Chem. Mater.* **2004**, *16*, 2814.
(23) Hogemann, D.; Ntziachristos, V.; Josephson, L.; Weissleder, R. *Bioconjugate Chem.* **2002**, *13*, 116.
(24) Sugimoto, T.; Matijeviæ, E. *J. Colloid Interface Sci.* **1980**, *74*, 227.
(25) Zhu, Y. F.; Zhao, W. R.; Chen, H. R.; Shi, J. L. *J. Phys. Chem. C* **2007**, *111*, 5281.
(26) Sun, S. H.; Zeng, H.; Robinson, D. B. *J. Am. Chem. Soc.* **2004**, *126*, 273.
(27) Gee, S. H.; Hong, Y. K.; Erickso, D. W.; Park, M. H. *J. Appl. Phys.* **2003**, *93*, 7560.
(28) Lyon, J. L.; Fleming, D. A.; Stone, M. B.; Schiffer, P.; Williams, M. E. *Nano Lett.* **2004**, *4*, 719.
(29) Sahoo, Y.; Cheon, M.; Wang, S.; Luo, H.; Furlani, E. P.; Prasad, P. N. *J. Phys. Chem. B* **2004**, *10*, 8–3380.
(30) Kim, S. W.; Kim, M.; Lee, W. Y.; Hyeon, T. *J. Am. Chem. Soc.* **2002**, *124*, 7642.
(31) Tan, B.; Rankin, S. E. *Langmuir* **2005**, *21*, 8180.
(32) Ding, Y.; Hu, Y.; Jiang, X.; Zhang, L.; Yang, C. *Angew. Chem., Int. Ed.* **2004**, *43*, 6369.
(33) Zhu, L. P.; Xiao, H. M.; Zhang, W. D.; Yang, Guo.; Fu, S. Y. *Cryst. Growth Des.* **2008**, *8*, 957.
(34) Lou, X. W.; Yuan, C.; Rhoades, E.; Zhang, Q.; Archer, L. A. *Adv. Funct. Mater.* **2006**, *16*, 1679.
(35) Chen, X. Y.; Zhang, Z. J.; Li, X. X.; Shi, C. W. *Chem. Phys. Lett.* **2006**, *422*, 294.
(36) Jia, B. P.; Gao, L. *J. Phys. Chem. C* **2008**, *112*, 666.
(37) Yu, D. B.; Sun, X. Q.; Zou, J. W.; Wang, Z. R.; Wang, F.; Tang, K. *J. Phys. Chem. B* **2006**, *110*, 21667.
(38) Li, X. H.; Zhang, D. H.; Chen, J. S. *J. Am. Chem. Soc.* **2006**, *128*, 8382.
(39) Deng, H.; Li, X.; Peng, Q.; Wang, X.; Chen, J.; Li, Y. D. *Angew. Chem., Int. Ed.* **2005**, *44*, 2782.
(40) Zhang, Y.; Li, Y. D. *J. Phys. Chem. B* **2004**, *108*, 17805.
(41) Yang, H. G.; Zeng, H. C. *J. Phys. Chem. B* **2004**, *108*, 3492.
(42) Liu, B.; Zeng, H. C. *Small* **2005**, 566.
(43) Wang, X.; Yuan, F. L.; Hu, P.; Yu, L. J.; Bai, L. Y. *J. Phys. Chem. B* **2008**, *112*, 8773.
(44) Hou, H. H.; Peng, Q.; Zhang, S. Y.; Guo, Q, X.; Xie, Y. *Eur. J. Inorg. Chem.* **2005**, 2625.
(45) Peng, Q.; Dong, Y. J.; Li, Y. D. *Angew. Chem., Int. Ed.* **2003**, *42*, 3027.

JP806406C